Proceedings of the 1st International Workshop on CFD and Biomass Thermochemical Conversion
Leipzig, Germany, 30 September 2014
Paper No. XXX (The number assigned to the abstract)

Transient simulations of biomass char gasification

Nils Erland L. Haugen
SINTEF Energy Research
Trondheim, Norway
nils.e.haugen@sintef.no

Jonas Kruger, Terese Løvås
Department of Energy and Process Engineering, Norwegian University of Science and Technology,
Trondheim, Norway
jonas.kruger@ntnu.no

Reginald E. Mitchell and Matthew B. Tilghman
Department of Mechanical Engineering, Stanford University, Stanford, USA
remitche@stanford.edu

ABSTRACT

Results of simulations of gasification of corn-stover char in environments similar to the ones established in a full scale gasification reactor are presented. The heterogeneous reaction mechanism employed in the model takes into account char gasification via CO_2 and H_2O as well as char oxidation via O_2 to account for the low levels of oxygen added to gasifiers to drive the endothermic gasification reactions. Reactions that account for CO and H_2 inhibition are included in the reaction mechanism. When H_2 and CO are not present in the ambient gas, the inhibition of the gasification rate is found *not* to be due to adsorbed H or CO species occupying carbon sites.

In the model, account is also made for radiation exchange between char particles and between particles and the surrounding wall. It is shown that for many applications, inter-particle radiation, which is neglected in most gasification models, can be quite significant in influencing the char-particle cooling rate.

KEYWORDS: Biomass, gasification, heterogeneous reactions, adsorbed species.

1 INTRODUCTION

The gasification process consists of the devolatilization phase, followed by reactions of the volatiles, and then the char burnout phase. The char burnout proceeds through heterogeneous reactions between the gas and the solid phase. Single particle char burnout can be modelled using transient, zero dimensional models, *i.e.* with no spatial discretization, which is done by *e.g.* Qiao *et al.* (2012) [1] and references therein. These zero dimensional models are fast and can potentially be used as sub-models for heterogeneous reactions in higher dimensional CFD tools.

In this work, gasification of biomass char is studied in a simulation code that includes a detailed heterogeneous reaction mechanism for char reactivity to CO_2, H_2O and O_2 and uses GRI-Mech 3.0 as the chemical kinetic mechanism that describes the impact of homogeneous reactions. The code is transient

and zero dimensional in space, and is designed to be used both as a stand-alone gasification/combustion code and as a sub-model for heterogeneous reactions of solid particles in a CFD code when the particle evolution is described by Lagrangian particle tracking as well as when an Eulerian-Eulerian methodology is chosen. A newly developed sub-model [2] that accounts for gradients inside the particle in the zero dimensional representation is used to determine the mode of combustion.

2 METHOD

Let V define a volume enclosed by the surface S, containing a gas mixture with a constant number of N_p embedded char particles. Let the surface S be impermeable such that there is no mass flux over S and let it be flexible such that the volume V is allowed to change in order to keep the gas pressure of the enclosed gas constant. The total mass inside S is then constant and equal to $m = m_p N_p + m_g$ where m_p is the mass of each particle while m_g is the mass of the gas. It is clear that the gas density is given by $\rho_g = m_g/V$ while the particle number density is $n_p = N_p/V$.

The heterogeneous particle-to-gas reactions are determined by the set of reactions listed in Table 1 [3], while the homogeneous gas phase reactions are determined by the GRI-3.0 reaction mechanism. The governing conservation equations for the gas phase are solved for the gas density, composition and temperature, while for the biomass char particles, the differential equations that describe the transport of mass and energy are solved to yield the particle mass, temperature and adsorbed species concentrations during char conversion. The effectiveness factor approach of Thiele [4] is used to account for the concentration gradients that exists inside char particles at high-temperatures and is also used in the mode of conversion sub-model in which the evolution of the particle radius and apparent density are handled by the method described in Haugen *et al*. (2014) [2]. The simulation code utilized in the current work is the same as previously described elsewhere [5,6].

Table 1 Heterogeneous reaction mechanism

	Reaction	Pre-Exponential	Activation Energy (kJ/mol)	Std Dev (kJ/mol)
R1	$2C_f + H_2O \leftrightarrow C(OH) + C(H)$	$7.3 \cdot 10^7$	106	
R2	$C(OH) + C_f \leftrightarrow C(O) + C(H)$	$1.5 \cdot 10^{12}$	150	
R3	$C(H) + C(H) \leftrightarrow H_2 + 2C_f$	$1.0 \cdot 10^{12}$	100	
R4	$C(O) + C_b \rightarrow CO + C_f$	$1.0 \cdot 10^{13}$	353	28
R5	$C(OH) + C_b \leftrightarrow HCO + C_f$	$1.0 \cdot 10^{13}$	393	28
R6	$C_b + C_f + C(H) + H_2O \leftrightarrow CH_3 + C(O) + C_f$	$1.0 \cdot 10^{13}$	300	
R7	$C_b + C_f + C(H) + H_2 \leftrightarrow CH_3 + 2C_f$	$1.0 \cdot 10^{13}$	300	
R8	$C_f + C(H) + CO \rightarrow HCO + 2C_f$	$1.0 \cdot 10^{13}$	300	
R9	$C(H) + C(H) \rightarrow CH_2 + C_f$	$3.0 \cdot 10^{11}$	426	
R10	$CO_2 + C_f \leftrightarrow C(O) + CO$	$8.6 \cdot 10^4$	188	
R11	$C_b + CO_2 + C(O) \rightarrow 2CO + C_f$	$3.26 \cdot 10^{12}$	367	
R12	$C(CO) \leftrightarrow CO + C_f$	$1.0 \cdot 10^{13}$	455	53
R13	$CO + C(CO) \rightarrow CO_2 + 2C_f$	$3.36 \cdot 10^6$	266	
R14	$2C_f + O_2 \rightarrow C(O) + CO$	$7.0 \cdot 10^{10}$	150	
R15	$2C_f + O_2 \rightarrow C_2(O_2)$	$3.0 \cdot 10^8$	103	
R16	$C_f + C_b + C(O) + O_2 \rightarrow CO_2 + C(O) + C_f$	$1.5 \cdot 10^7$	78	
R17	$C_f + C_b + C(O) + O_2 \rightarrow CO + 2C(O)$	$2.1 \cdot 10^7$	103	
R18	$C_b + C_2(O_2) \rightarrow CO_2 + 2C_f$	$1.0 \cdot 10^{13}$	304	33

3 RESULTS

In the following discussion, simulations of corn stover char particles exposed to the conditions given in Table 2 are presented. When comparing results of simulations, these conditions and the full reaction mechanism shown in Table 1 define the base case simulation.

Table 2 Properties of the simulations

Property	Value	Units
Carbon to gas mass ratio	0.4	-
Particle radius	50	μm
Particle number density	10^9	m^{-3}
Pressure	24	bar
Initial temperature	1640	K
Reactor size	1	m
Initial mass fraction of H_2O	0.6	-
Initial mass fraction of O_2	0.29	-
Initial mass fraction of CO_2	0.1	-
Initial mass fraction of N_2	0.01	-

From Figure 1, it can be seen that for the base case simulation (black line) full conversion is reached after about 2.4 seconds, while the peak particle and gas temperatures reach 2450 K and 2800 K, respectively. In order to investigate the effect of H_2 inhibition on the heterogeneous reactions, reactions R3 reverse and R7 forward are turned off by temporarily setting their pre-exponential factors to zero. By this approach all other aspects of the simulations, *e.g.* transport data and gas phase reactions, are kept un-changed. These results are presented by the red lines in Figure 1, which show that full conversion is reached slightly earlier than for the base case. A weak temperature dependence is also observed. This means that there is indeed some inhibition of the heterogeneous reactions due to the hydrogen present in the gas phase, but the effect is not very strong. Inhibition due to CO can be examined in the same manner, by turning off reactions R8, R10 reverse, R12 reverse and R13. This is visualized by the blue line in Figure 2. Like for H_2 inhibition, it can be seen that CO does inhibit the reactions by yielding full conversion in a shorter time than the base case, but the effect is still not very strong.

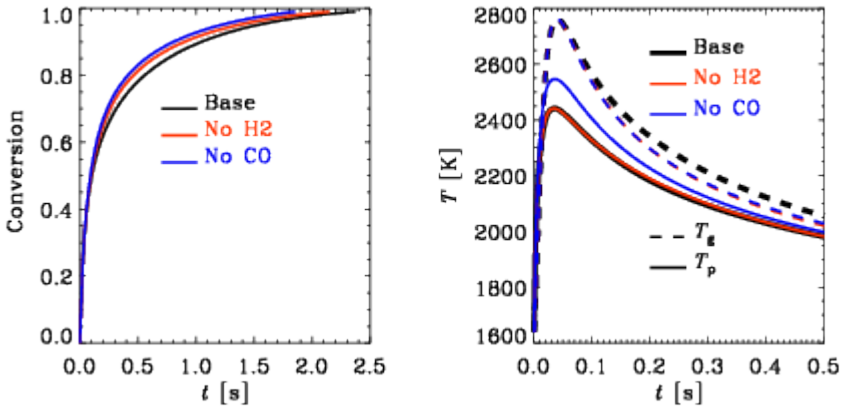

Figure 1 Conversion (left panel) and particle and gas temperatures (right panel) as a function of time for the base case (black line), the case with no H_2 heterogeneous reactants (red line) and the case with no CO heterogeneous reactants (blue line).

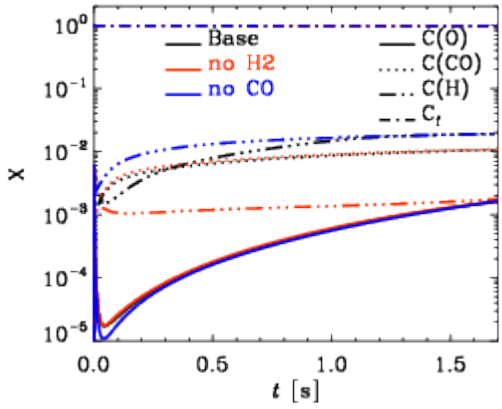

Figure 2 Surface coverage fractions of adsorbed species as a function of time. The solid line represents adsorbed oxygen, the dotted line adsorbed CO and the dashed-triple-dotted line adsorbed H, while the dashed-dotted line represents the free carbon sites.

In Figure 2 the fraction of adsorbed species on the surface is shown for the base case (black lines) together with the cases with no H_2 reactions (red lines) and no CO reactions (blue lines). The amount of H adsorbed on the surface is found to decrease strongly when the hydrogen reactions are neglected. In the same way, the amount of adsorbed CO vanishes when CO reactions are neglected. It is clear however, that due to the low fraction of surface sites being occupied by adsorbed species, the fraction of available sites (C_f) is always close to unity. This means that both H_2 and CO inhibition must be due to a change in the reverse rates of these heterogeneous reactions, and *not* due to adsorbed species filling up the free sites and by this "clogging" the heterogeneous reaction paths.

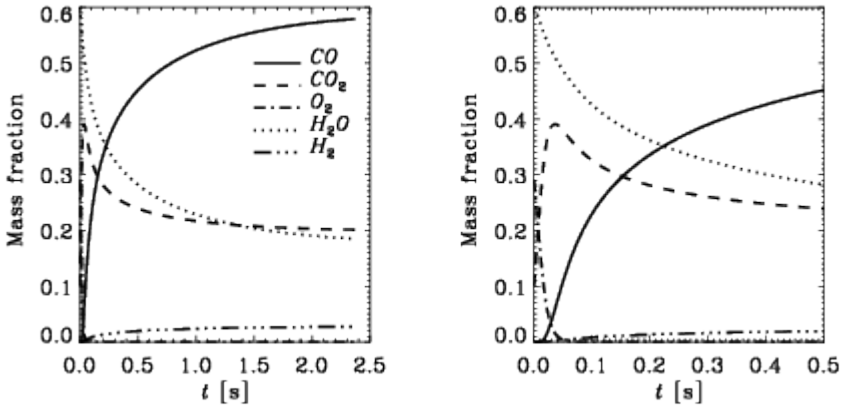

Figure 3 Mass fraction of gas phase species (ambient) as a function of time for the base case.

The mass fraction of the species in the ambient are shown in Figure 3, where one can see that the mass fraction of CO reaches almost 0.6. From the right plot it can be seen that the mass fraction of CO_2 starts to decrease when the O_2 mass fraction reaches zero. By comparison with the right hand plot of Figure 1, the time when O_2 has been consumed is also found to roughly correspond to the time when the gas and particle temperatures start to decrease.

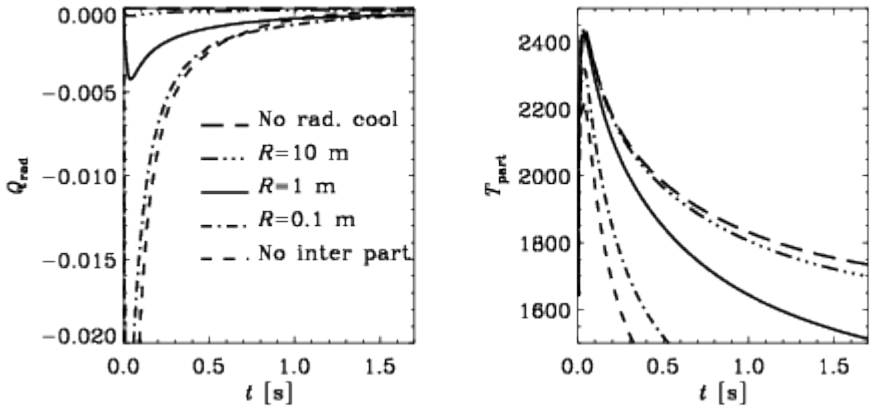

Figure 4: Radiative cooling of particles (left panel) and particle temperature (right panel) as a function of time for different treatments of radiation and reactor sizes.

It is common to see that particle-particle radiation is neglected for gasification environments. For the conditions presented here (see Table 2) the radiative particle cooling is represented by the solid line in the left panel of Figure 4. If inter particle radiation is neglected, it can be seen by the dashed line that the radiative cooling increases strongly, and is a good approximation only for reactors of sizes less than 10 cm (dashed-dotted line). When increasing the reactor size to 10 m (dashed-triple-dotted line) the radiative cooling becomes very low and approaches the situation when radiative cooling is neglected. The reason behind this is that for large reactors the optical depth is larger than unity for the majority of the particle cloud. This means that just a small fraction of the radiation emitted from the particles reaches the reactor walls. In the right hand panel of Figure 4, the particle temperature is shown to vary strongly with the reactor size and particle radiation model. As expected, the larger reactor sizes yields higher temperatures.

4 CONCLUSION

It is found that for the conditions used in this paper, there is inhibition of the gasification rate due to both hydrogen and carbon monoxide. The inhibition is not very strong at the high temperatures studied. It is concluded that in the absence of H_2 and CO in the gas phase, inhibition is *not* due to adsorbed H or CO filling up the free carbon sites for there are ample free sites available.

It is also found that for large enough reactors, it is crucial to include particle-particle radiation in the energy transport equation. Particle-particle radiation can be neglected only when the entire volume has an optical depth well below unity. For very large particle enclosures, the neglect of radiative cooling is an adequate assumption.

5 ACKNOWLEDGEMENTS

This work forms part of the CAMPS project supported by the Research Council of Norway (215707). The work has additionally been produced with support from the BIGCCS Centre, performed under the Norwegian Research Program Centres for Environment-Friendly Energy Research (FME). The authors acknowledge the following partners for their contributions: Aker Solutions, ConocoPhillips, Gassco, Shell, Statoil, TOTAL, GDF SUEZ and the Research Council of Norway (193816/S60).

The research leading to these results has received funding from the Polish-Norwegian Research Programme operated by the National Centre for Research and Development under the Norwegian Financial Mechanism 2009-2014 in the frame of Project Contract No Pol-Nor/232738/101/2014

NELH also acknowledges the Research Council of Norway under the FRINATEK grant 231444.

REFERENCES

[1] L. Qiao, J. Xu, A. Sane and J. Gore, Combustion and Flame **159**, 1693 (2012).

[2] N. E. L. Haugen, M. Tilghman and R. E. Mitchell, Combustion and Flame **161**, 612 (2014).

[3] M. Tilghman and R. E. Mitchell, "Coal and Biomass Char Reactivities in Gasification and Combustion Environments", Submitted for publication in Combustion & Flame, May 2014

[4] E. W. Thiele, Ind. Eng. Chem **31**, 916 (1939)

[5] N. E. L. Haugen, R. E. Mitchell and M. Tilghman, 8th US National Combustion Meeting, May 19-22, 2013.

[6] N. E. L. Haugen, R. E. Mitchell and M. Tilghman, "A comprehensive model for char particle conversion in environments containing O_2 and CO_2", Submitted for publication in Combustion & Flame, August 2014